

Verified Task-Space Motion Planning Under Joint-Space Constraints

Hanjiang Hu, Changliu Liu, Yebin Wang

Abstract—Reactive task-space planners such as Bug2 operate with fixed Cartesian step sizes and are unaware of the manipulator’s joint-angle limits. When the Jacobian is poorly conditioned, even small Cartesian steps can demand joint changes that exceed admissible bounds; clipping the joints to their limits causes tracking drift and can prevent goal reaching entirely. We address this by computing, at each planning step, the largest Cartesian hyperrectangle that is *certifiably reachable* under joint displacement bounds. Using a second-order polynomial approximation of the inverse kinematics and the S-procedure, we formulate a small semidefinite program whose solution yields the certified half-width λ^* . An equivalent bisection procedure exploiting the quadratic structure solves the certification in sub-millisecond time. Integrating this certificate with Bug2 yields a planner whose step size adapts to local kinematic conditioning. In a statistical evaluation over 94 adversarial scenarios spanning six joint-limit settings, the SOS-verified planner achieves zero joint-limit violations with a 100% goal-reaching rate, whereas a standard Bug2 planner violates joint limits in 6–11% of steps and fails to reach the goal in up to 18% of scenarios.

I. INTRODUCTION

A fundamental challenge in robotic motion planning is the mismatch between the *task space*, where goals and obstacles are naturally specified, and the *joint space*, where the robot’s physical constraints reside. High-level planners often generate Cartesian trajectories under the implicit assumption that an inverse kinematics (IK) solution exists at every waypoint, an assumption that can fail when joint-angle limits, velocity bounds, or kinematic singularities are present [1], [2]. In safety-critical applications such as industrial manipulation and human–robot collaboration, violating these constraints is not merely suboptimal but potentially hazardous.

Existing approaches to joint-aware task-space motion can be broadly categorized as *integrated* or *hierarchical*. Integrated methods plan directly in joint space while enforcing task-space requirements: sampling-based planners project random configurations onto task-constraint manifolds [3], [4], and trajectory optimizers jointly minimize cost subject to task and joint constraints [5], [6], which may fail to find a feasible solution if starting from a poor initial guess. Hierarchical methods first plan a path in task space and then resolve each waypoint to joint space via inverse kinematics, typically using the Jacobian pseudoinverse or its damped variants [1], [7]. Reactive planners such as the Bug family [8] are a prominent instance of the hierarchical paradigm: they compute task-space directions online and rely on local IK

to execute each step. We focus on the hierarchical setting because it is the natural framework for reactive and online planning in partially known environments, where task-space goals and obstacle geometry are discovered incrementally. The central vulnerability of this paradigm is that a fixed Cartesian step size that is safe at one configuration may violate joint limits at another, due to the configuration-dependent amplification $\|\Delta\theta\| \leq \|\Delta z\|/\sigma_{\min}(J(\theta))$. Clipping the joints to their limits causes the end-effector to land at an unintended position, producing cumulative tracking drift.

This paper addresses the question: *given a robot’s current joint configuration and per-step joint displacement bounds, what is the largest Cartesian region that is guaranteed to be reachable?* If such a *certified reachable set* can be computed efficiently at each planning step, it can serve as a feasibility filter for any task-space planner, ensuring that every commanded Cartesian displacement admits a valid joint-space realization. Fig. 1 illustrates the idea: prior SOS-based methods in robotics [9], [10] certify regions in *state/joint space* where a closed-loop controller keeps the system within a collision-free funnel, whereas our method certifies a region in *task space* that is kinematically reachable from the current joint configuration under displacement bounds.

We answer this question using Sum-of-Squares (SOS) programming [11]. Specifically, we construct a second-order polynomial approximation of the inverse kinematics around the current configuration, and formulate an SOS optimization that maximizes the half-width λ^* of a Cartesian hyperrectangle subject to the constraint that the polynomial IK maps every point in the hyperrectangle to joint displacements within bounds. The S-procedure [12], [13] provides a computationally tractable sufficient condition via a small semidefinite program. Since the polynomial IK is quadratic, the resulting SOS relaxation is exact (lossless) for our problem.

We integrate this certified reachable set with the Bug2 reactive planner [8], yielding a planner that *adapts* its Cartesian step size to the local kinematic conditioning. In regions of high $\kappa(J)$, the certified set λ^* automatically shrinks and the planner takes smaller steps; in well-conditioned regions, it takes larger steps. Every step is guaranteed to satisfy joint limits by construction, eliminating clipping-induced drift entirely. Note that while we demonstrate the approach with Bug2, the certified reachable set is a general-purpose feasibility filter that can be extended to any hierarchical task-space planner, to provide per-step joint-feasibility guarantees. The contributions are listed below.

- An SOS-based method to compute the maximal certified Cartesian reachable hyperrectangle from any joint

H. Hu and C. Liu are with the Robotics Institute, Carnegie Mellon University. This work was done while H. Hu was a research intern at Mitsubishi Electric Research Laboratories (MERL), Cambridge, MA 02139, USA. (email: hanjianghu@cmu.edu).

Y. Wang is with the MERL. (email: yebinwang@ieee.org).

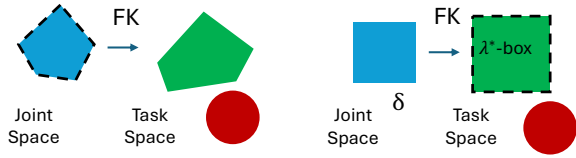


Fig. 1: **Left:** Prior methods certify collision-free regions in joint/state space (dashed-line) where a controller keeps the system within a safe funnel. **Right:** This work certifies a region in *task space* (dashed-line λ^* -box) that is guaranteed reachable from the current joint configuration under joint displacement bounds δ . The certified box serves as a per-step feasibility filter for any task-space planner.

configuration under per-step joint displacement bounds (Section IV-B);

- Integration with the Bug2 reactive planner, yielding an adaptive-step algorithm with per-step joint-feasibility guarantees (Section IV-C);
- A computationally efficient bisection implementation that exploits the quadratic structure of the polynomial IK, providing equivalent certificates to the full SOS program in sub-millisecond time (Section IV-D);
- A statistical evaluation across 94 adversarial scenarios and six joint-limit settings, demonstrating zero joint-limit violations and 100% goal reaching where vanilla Bug2 fails (Section V).

II. RELATED WORK

Integrated task-constrained planning: Integrated methods plan directly in joint space while enforcing task-space requirements. Stilman [3] introduced tangent-space sampling and first-order retraction for RRT-based planning on constraint manifolds. Kingston et al. [4], [14] unified these techniques in the IMACS framework, showing that various constraint-adherence methods compose with standard sampling-based planners. Trajectory optimization approaches [5], [6], [15] jointly optimize over the full trajectory subject to task, joint, and collision constraints. These methods are effective for offline or batch planning but do not provide per-step kinematic feasibility certificates that a reactive planner could use online.

Hierarchical task-space planning: Hierarchical methods first compute a task-space path and then resolve each waypoint to joint space via IK. The Jacobian pseudoinverse and its damped variants [1], [16], [17] are the standard IK mechanism; they improve robustness near singularities but offer no formal guarantee that joint limits are respected. Variable step-size strategies [7] adapt the IK step heuristically for convergence speed but do not certify joint-limit satisfaction. Reactive planners—Bug algorithms [8], potential fields [18]—are canonical instances of the hierarchical paradigm, prized for online operation, but oblivious to joint-space constraints. Our work adds a certified feasibility layer to this paradigm, certifying regions of *task space* that are kinematically reachable under joint constraints, a complementary notion suited to task-space planning. Fig. 1 contrasts the two settings.

III. PROBLEM FORMULATION

We denote by $\|\cdot\|$ the Euclidean norm and by $\|\cdot\|_\infty$ the infinity norm. For a symmetric matrix $M \in \mathbb{R}^{d \times d}$, we write $M \succeq 0$ to indicate positive semidefiniteness. The set $\Sigma[y]$ denotes the cone of SOS polynomials in variables y , i.e., $p \in \Sigma[y]$ if and only if $p(y) \geq 0$ for all y and p admits a decomposition $p = \sum_j q_j^2$ for some polynomials q_j . The singular values of a matrix M are $\sigma_1 \geq \dots \geq \sigma_r > 0$, and the condition number is $\kappa(M) = \sigma_1/\sigma_r$.

A. Planar Robot Model

Consider an n -link planar revolute manipulator with link lengths $\ell_1, \dots, \ell_n > 0$. The joint configuration is $\theta = (\theta_1, \dots, \theta_n)^\top \in \mathbb{R}^n$, and the forward kinematics (FK) map $\text{FK} : \mathbb{R}^n \rightarrow \mathbb{R}^2$ maps joint angles to the end-effector position in the plane. While we present the formulation for a planar manipulator with $\text{FK} : \mathbb{R}^n \rightarrow \mathbb{R}^2$ for notational clarity, the method generalizes to spatial manipulators with $\text{FK} : \mathbb{R}^n \rightarrow \mathbb{R}^m$ ($m \leq 6$): the polynomial IK approximation (11) extends naturally to m -dimensional task space, and the SOS certificate (21) involves $(m+1) \times (m+1)$ matrices (see Remark 2). The planar case is representative of SCARA-type manipulators, planar parallel mechanisms, and the in-plane motion of spatial arms constrained to a vertical plane (e.g., sagittal-plane reaching). The forward kinematics is

$$\mathbf{z} = \text{FK}(\boldsymbol{\theta}) = \begin{pmatrix} \sum_{i=1}^n \ell_i \cos \theta_i \\ \sum_{i=1}^n \ell_i \sin \theta_i \end{pmatrix}, \quad (1)$$

where $\mathbf{z} = (z_1, z_2)^\top \in \mathbb{R}^2$ is the end-effector position in the task (Cartesian) space $\mathcal{W} \subset \mathbb{R}^2$. The manipulator Jacobian is

$$\mathbf{J}(\boldsymbol{\theta}) = \frac{\partial \text{FK}}{\partial \boldsymbol{\theta}} \in \mathbb{R}^{2 \times n}, \quad \mathbf{J}_{ki} = \begin{cases} -\ell_i \sin \theta_i, & k = 1, \\ \ell_i \cos \theta_i, & k = 2. \end{cases} \quad (2)$$

B. Joint-Limit Constraints

In many applications, the joint displacement per planning step is bounded. These bounds arise from physical joint-angle limits of the actuators, velocity or torque limits (which, for a fixed planning rate Δt , translate to maximum angular displacements $\delta_i = \dot{\theta}_{i,\max} \Delta t$), or safety constraints imposed by the operating environment (e.g., collaborative workspaces where large joint motions are restricted to limit the robot's swept volume). Formally, at each planning step the change in joint angles from the current configuration $\boldsymbol{\theta}^{(t)}$ must satisfy

$$|\theta_i^{(t+1)} - \theta_i^{(t)}| \leq \delta_i, \quad i = 1, \dots, n, \quad (3)$$

where $\boldsymbol{\delta} = (\delta_1, \dots, \delta_n)^\top > \mathbf{0}$ are given bounds. We denote the admissible joint displacement set at configuration $\boldsymbol{\theta}^{(t)}$ by

$$\Theta(\boldsymbol{\theta}^{(t)}, \boldsymbol{\delta}) := \{\boldsymbol{\theta} \in \mathbb{R}^n : |\theta_i - \theta_i^{(t)}| \leq \delta_i, i = 1, \dots, n\}. \quad (4)$$

When all bounds are equal ($\delta_i = \delta$ for all i), this reduces to $\|\boldsymbol{\theta} - \boldsymbol{\theta}^{(t)}\|_\infty \leq \delta$.

C. Task-Space Planning Problem

Let $\mathbf{z}_{\text{start}} = \text{FK}(\boldsymbol{\theta}^{(0)})$ be the initial end-effector position and $\mathbf{z}_{\text{goal}} \in \mathcal{W}$ the desired target. The workspace contains a set of obstacles $\mathcal{O} = \bigcup_{j=1}^{N_{\text{obs}}} \mathcal{O}_j \subset \mathcal{W}$.

Problem 1 (Joint-Limited Task-Space Planning): Find a sequence of joint configurations $\{\boldsymbol{\theta}^{(t)}\}_{t=0}^T$ such that:

- 1) **Goal reaching:** $\|\text{FK}(\boldsymbol{\theta}^{(T)}) - \mathbf{z}_{\text{goal}}\| \leq \epsilon_{\text{tol}}$;
- 2) **Joint feasibility:** $\boldsymbol{\theta}^{(t+1)} \in \Theta(\boldsymbol{\theta}^{(t)}, \boldsymbol{\delta})$ for all $t = 0, \dots, T-1$;
- 3) **Obstacle avoidance:** $\text{FK}(\boldsymbol{\theta}^{(t)}) \notin \mathcal{O}$ for all t (end-effector collision avoidance; full-body collision checking can be incorporated by inflating the obstacles to account for the link geometry, which is standard for low-DOF planar arms [2]).

D. Challenge: Kinematic Coupling

A standard approach is to plan a Cartesian path and convert each waypoint to a joint-space configuration via the pseudoinverse mapping $\Delta\boldsymbol{\theta} = J(\boldsymbol{\theta})^\dagger \Delta\mathbf{z}$, where each Cartesian step $\Delta\mathbf{z}$ is chosen with a fixed magnitude s . The difficulty is that

$$\|\Delta\boldsymbol{\theta}\| \leq \|J^\dagger\| \cdot \|\Delta\mathbf{z}\| = \frac{\|\Delta\mathbf{z}\|}{\sigma_{\min}(J)}, \quad (5)$$

where $\sigma_{\min}(J)$ is the smallest singular value. The condition number $\kappa(J) = \sigma_{\max}/\sigma_{\min}$ varies across the workspace: in high- κ regions, even small Cartesian displacements can require joint changes exceeding $\boldsymbol{\delta}$. A fixed Cartesian step size $s = \delta/\kappa(\boldsymbol{\theta}^{(0)})$ that is safe at the initial configuration may violate (3) when κ increases along the path.

A natural idea is to update the step size at each step using the current condition number, i.e., $s^{(t)} = \delta/\kappa(\boldsymbol{\theta}^{(t)})$. However, this heuristic has two limitations. First, it uses only the *worst-case singular-value bound* (5), which can be overly conservative since it does not account for the direction of $\Delta\mathbf{z}$ relative to the singular vectors of J . Second, it relies on a linear (first-order) IK model, ignoring the quadratic and higher-order terms that become significant in poorly-conditioned regions. Variable step-size strategies for iterative IK have been explored in [7], but these adapt the step heuristically for convergence speed rather than providing formal joint-limit certificates. In contrast, our SOS-based approach computes λ^* by certifying the *exact* quadratic polynomial IK over the full Cartesian box, providing a tight and formally guaranteed bound. Clipping the joint displacement to $\pm\boldsymbol{\delta}$ produces a *different* end-effector position than intended, causing cumulative Cartesian tracking drift.

IV. METHOD

Our approach has three components: (i) a second-order polynomial approximation of the local inverse kinematics, (ii) an SOS-based certification of the maximal Cartesian reachable set under joint limits, and (iii) integration with the Bug2 reactive planner. Components (i)–(ii) address the core limitation of existing task-space planners: they provide a *certified* answer to the question “how far can the end-effector move while guaranteeing joint feasibility?” The

polynomial approximation (i) captures the nonlinear coupling between task and joint space that first-order (Jacobian-only) methods miss, while the SOS certificate (ii) provides a formal guarantee over the *entire* Cartesian box rather than a single-direction worst-case bound. Component (iii) demonstrates the utility of these certificates in a concrete planning setting.

A. Polynomial Inverse Kinematics

At the current configuration $\boldsymbol{\theta}_0 := \boldsymbol{\theta}^{(t)}$ with end-effector position $\mathbf{z}_0 = \text{FK}(\boldsymbol{\theta}_0)$, we seek a polynomial map $\hat{\boldsymbol{\theta}} : \mathbb{R}^2 \rightarrow \mathbb{R}^n$ such that $\hat{\boldsymbol{\theta}}(\Delta\mathbf{z}) \approx \text{IK}(\mathbf{z}_0 + \Delta\mathbf{z})$ for small displacements $\Delta\mathbf{z} = (\Delta z_1, \Delta z_2)^\top$.

1) *First-Order Term:* The linear approximation uses the Moore–Penrose pseudoinverse:

$$\hat{\boldsymbol{\theta}}^{(1)}(\Delta\mathbf{z}) = \boldsymbol{\theta}_0 + A \Delta\mathbf{z}, \quad A := J(\boldsymbol{\theta}_0)^\dagger \in \mathbb{R}^{n \times 2}. \quad (6)$$

2) *Second-Order Term:* To capture nonlinear IK behavior, we augment with quadratic terms. Define the correction matrix for joint i :

$$B_i = \begin{pmatrix} b_{i,11} & b_{i,12}/2 \\ b_{i,12}/2 & b_{i,22} \end{pmatrix} \in \mathbb{R}^{2 \times 2}, \quad (7)$$

where the coefficients capture how J^\dagger varies along the IK manifold. These are computed via finite differences of J^\dagger evaluated at perturbed configurations $\boldsymbol{\theta}_0 + A\mathbf{e}_k h$ for small $h > 0$:

$$b_{i,11} = \frac{1}{2h} ([J^\dagger(\boldsymbol{\theta}_0 + A\mathbf{e}_1 h)]_{i1} - A_{i1}), \quad (8)$$

$$b_{i,22} = \frac{1}{2h} ([J^\dagger(\boldsymbol{\theta}_0 + A\mathbf{e}_2 h)]_{i2} - A_{i2}), \quad (9)$$

$$b_{i,12} = \frac{1}{h} ([J^\dagger(\boldsymbol{\theta}_0 + A\mathbf{e}_1 h)]_{i2} - A_{i2}). \quad (10)$$

The full second-order polynomial IK for joint i is then

$$\hat{\boldsymbol{\theta}}_i(\Delta\mathbf{z}) = \boldsymbol{\theta}_{0,i} + A_{i1}\Delta z_1 + A_{i2}\Delta z_2 + b_{i,11}\Delta z_1^2 + b_{i,12}\Delta z_1\Delta z_2 + b_{i,22}\Delta z_2^2. \quad (11)$$

3) *Approximation Error Bound:* Let $\varepsilon(\rho)$ denote the worst-case approximation error over the Cartesian box $[-\rho, \rho]^2$:

$$\varepsilon(\rho) := \max_{\|\Delta\mathbf{z}\|_\infty \leq \rho} \|\text{FK}(\hat{\boldsymbol{\theta}}(\Delta\mathbf{z})) - (\mathbf{z}_0 + \Delta\mathbf{z})\|. \quad (12)$$

This is evaluated numerically on a dense grid (we use a 7×7 grid, requiring 49 forward-kinematics evaluations per step—negligible compared to the bisection cost). The effective joint bounds used for certification are then

$$\delta_i^{\text{eff}} := \delta_i - \varepsilon(\rho), \quad i = 1, \dots, n. \quad (13)$$

We clarify the role of $\varepsilon(\rho)$: it bounds the *task-space* error of the polynomial IK model, i.e., the gap between the target Cartesian position and the actual position achieved by the polynomial IK joint angles. Since $\varepsilon(\rho)$ also bounds the maximum *joint-space* error $\|\hat{\boldsymbol{\theta}}(\Delta\mathbf{z}) - \boldsymbol{\theta}^{\text{true}}\|_\infty$ (via the Jacobian), subtracting it from the joint bounds ensures that the true IK solution—not just the polynomial approximation—respects (3). We assume the Jacobian is non-singular to avoid finding ρ which gives a small ε . More precisely, if the polynomial IK predicts a joint displacement $\Delta\hat{\boldsymbol{\theta}}_i$ and the

true displacement is $\Delta\theta_i^{\text{true}}$, then $|\Delta\hat{\theta}_i - \Delta\theta_i^{\text{true}}| \leq C \cdot \varepsilon(\rho)$ where C depends on the local Jacobian; the reduction $\delta_i^{\text{eff}} = \delta_i - \varepsilon(\rho)$ conservatively accounts for this gap. If $\delta_i^{\text{eff}} \leq 0$ for any i , the polynomial approximation is too coarse and ρ must be reduced.

B. SOS-Based Reachable Set Certification

We now formulate the core certification problem: given the polynomial IK (11) and effective joint bounds δ^{eff} , find the largest $\lambda > 0$ such that

$$\forall \Delta \mathbf{z} \in [-\lambda, \lambda]^2 : |\hat{\theta}_i(\Delta \mathbf{z}) - \theta_{0,i}| \leq \delta_i^{\text{eff}}, \quad i = 1, \dots, n. \quad (14)$$

1) *Quadratic Form Representation:* Define the monomial vector $\mathbf{y} = (1, \Delta z_1, \Delta z_2)^\top$. The polynomial IK displacement for joint i can be written as

$$\Delta\hat{\theta}_i(\Delta \mathbf{z}) = \hat{\theta}_i(\Delta \mathbf{z}) - \theta_{0,i} = \mathbf{y}^\top Q_i \mathbf{y}, \quad (15)$$

where

$$Q_i = \begin{pmatrix} 0 & A_{i1}/2 & A_{i2}/2 \\ A_{i1}/2 & b_{i,11} & b_{i,12}/2 \\ A_{i2}/2 & b_{i,12}/2 & b_{i,22} \end{pmatrix} \in \mathbb{S}^3. \quad (16)$$

The constraint (14) decomposes into $2n$ scalar polynomial nonpositivity conditions. For each joint i and sign $\sigma \in \{+1, -1\}$:

$$p_{i,\sigma}(\Delta \mathbf{z}) := \sigma \cdot \mathbf{y}^\top Q_i \mathbf{y} - \delta_i^{\text{eff}} \leq 0, \quad \forall \Delta \mathbf{z} \in [-\lambda, \lambda]^2. \quad (17)$$

2) *S-Procedure Relaxation:* The domain constraint $\Delta \mathbf{z} \in [-\lambda, \lambda]^2$ is encoded via two nonnegative polynomials:

$$\begin{aligned} g_1(\Delta \mathbf{z}) &= \lambda^2 - \Delta z_1^2 \geq 0, & (18) \\ g_2(\Delta \mathbf{z}) &= \lambda^2 - \Delta z_2^2 \geq 0. & (19) \end{aligned}$$

In the \mathbf{y} -basis, these are $g_k(\Delta \mathbf{z}) = \mathbf{y}^\top G_k(\lambda) \mathbf{y}$ with

$$G_1 = \begin{pmatrix} \lambda^2 & 0 & 0 \\ 0 & -1 & 0 \\ 0 & 0 & 0 \end{pmatrix}, \quad G_2 = \begin{pmatrix} \lambda^2 & 0 & 0 \\ 0 & 0 & 0 \\ 0 & 0 & -1 \end{pmatrix}. \quad (20)$$

By the generalized S-procedure [12], [13], a sufficient condition for (17) is:

Proposition 1 (S-Procedure Certificate): The constraint $p_{i,\sigma}(\Delta \mathbf{z}) \leq 0$ for all $\Delta \mathbf{z} \in [-\lambda, \lambda]^2$ holds if there exist multipliers $c_1, c_2 \geq 0$ such that

$$-\sigma \cdot Q_i + \delta_i^{\text{eff}} \cdot E_{11} + c_1 G_1(\lambda) + c_2 G_2(\lambda) \succeq 0, \quad (21)$$

where $E_{11} = \text{diag}(1, 0, 0)$.

Proof: Multiplying $g_k \geq 0$ by $c_k \geq 0$ and summing gives $\sum_k c_k g_k(\Delta \mathbf{z}) \geq 0$ on the domain. Adding to $-p_{i,\sigma}(\Delta \mathbf{z}) = -\sigma \cdot \mathbf{y}^\top Q_i \mathbf{y} + \delta_i^{\text{eff}}$ yields $\mathbf{y}^\top S \mathbf{y} \geq 0$ with S as in (21). If $S \succeq 0$, then $-p_{i,\sigma}(\Delta \mathbf{z}) \geq 0$, i.e., $p_{i,\sigma}(\Delta \mathbf{z}) \leq 0$, as required. ■

3) *Optimization Problem:* The maximal certified Cartesian half-width λ^* is the solution of:

$$\lambda^* = \max_{\lambda, c_1^{(i,\sigma)}, c_2^{(i,\sigma)}} \lambda \quad (22a)$$

$$\text{s.t. } S_{i,\sigma}(\lambda, c_1, c_2) \succeq 0, \quad \forall i, \sigma, \quad (22b)$$

$$c_1^{(i,\sigma)}, c_2^{(i,\sigma)} \geq 0, \quad (22c)$$

$$0 \leq \lambda \leq \lambda_{\text{max}}, \quad (22d)$$

where

$$S_{i,\sigma} := -\sigma Q_i + \delta_i^{\text{eff}} E_{11} + c_1 G_1(\lambda) + c_2 G_2(\lambda). \quad (23)$$

This is a bilinear SDP in (λ, c_1, c_2) due to the $c_k \lambda^2$ terms in $c_k G_k(\lambda)$. For a fixed λ , (22) reduces to a standard SDP feasibility problem. We solve (22) via nonlinear programming with the positive semidefiniteness condition enforced through the Sylvester criterion (all leading principal minors ≥ 0):

$$[S]_{11} \geq 0, \quad (24)$$

$$[S]_{11}[S]_{22} - [S]_{12}^2 \geq 0, \quad (25)$$

$$\det(S) \geq 0. \quad (26)$$

Theorem 1 (Certified Reachable Set): If $\lambda^* > 0$ is a feasible solution of (22) at configuration θ_0 , then for every $\Delta \mathbf{z} \in [-\lambda^*, \lambda^*]^2$, the polynomial IK (11) produces joint displacements satisfying $|\Delta\hat{\theta}_i| \leq \delta_i^{\text{eff}} \leq \delta_i$ for all i . Consequently, the Cartesian box

$$\mathcal{R}(\theta_0) := \{z_0 + \Delta \mathbf{z} : \|\Delta \mathbf{z}\|_\infty \leq \lambda^*\} \quad (27)$$

is a verified inner approximation of the set of end-effector positions reachable from θ_0 under joint limits δ .

Proof: By Proposition 1, feasibility of (22) implies $|\mathbf{y}^\top Q_i \mathbf{y}| \leq \delta_i^{\text{eff}}$ for all $\Delta \mathbf{z} \in [-\lambda^*, \lambda^*]^2$ and all i . By (15), this gives $|\Delta\hat{\theta}_i(\Delta \mathbf{z})| \leq \delta_i^{\text{eff}}$. Since $\delta_i^{\text{eff}} = \delta_i - \varepsilon(\rho) \leq \delta_i$, the true IK displacement also satisfies the original bounds (3) up to the approximation error already subtracted. ■

Remark 1 (Exactness for Quadratics): Since the constraint polynomial $p_{i,\sigma}$ in (17) and the domain polynomials g_1, g_2 in (18)–(19) are all quadratic, the S-procedure relaxation is exact (lossless) for quadratic polynomials over quadratic domains [12].

Remark 2 (Generalization to Higher Dimensions): For a spatial manipulator with FK : $\mathbb{R}^n \rightarrow \mathbb{R}^m$ ($m \leq 6$), the monomial vector becomes $\mathbf{y} = (1, \Delta z_1, \dots, \Delta z_m)^\top \in \mathbb{R}^{m+1}$, the polynomial IK matrix $Q_i \in \mathbb{S}^{m+1}$, and the domain is encoded by m box constraints $g_k = \lambda^2 - \Delta z_k^2 \geq 0$. The S-procedure certificate is an $(m+1) \times (m+1)$ PSD condition with m multipliers. The bisection procedure generalizes directly: the grid becomes m -dimensional, and the Pataki–Barvinok rank bound still ensures SDP exactness provided the number of affine constraints $(m+1)$ satisfies $r(r+1)/2 \leq m+1$, i.e., $r \leq 1$. For $m \leq 6$, this is a small SDP and remains computationally tractable.

C. Integration with Bug2 Planner

The Bug2 algorithm [8] alternates between two modes: *go-to-goal* (GTG), moving directly toward the target, and *boundary-follow* (BF), circumnavigating an obstacle until the start–goal line is crossed closer to the goal. The standard Bug2 uses a fixed Cartesian step and is unaware of joint limits. We modify it with an adaptive step size driven by the certified reachable set.

We emphasize that the adaptive step-size mechanism and the polynomial IK update are not specific to Bug2: they can be used with any task-space planner that produces a desired Cartesian displacement direction $\mathbf{d}^{(t)}$ at each step. We choose Bug2 because (a) its fixed-step structure makes the failure mode under joint limits most transparent, and (b) its completeness guarantee (for point robots in the plane) transfers to our setting whenever $\lambda^* > 0$ everywhere along the path.

1) *Guaranteed Properties*: Before describing the algorithm, we state its key properties.

Proposition 2 (Per-Step Feasibility): If $\lambda^* > 0$ at step t , then $\boldsymbol{\theta}^{(t+1)} \in \Theta(\boldsymbol{\theta}^{(t)}, \boldsymbol{\delta})$.

Proof: Immediate from Theorem 1 and the construction (28) ensuring $\Delta \mathbf{z}^{(t)} \in [-\lambda^*, \lambda^*]^2$. ■

Remark 3 (Monotone Approach in GTG and Completeness): In GTG mode with no obstacle intersection, the distance to goal decreases by at least $\alpha \lambda^* \cos \phi$ per step, where ϕ is the angle between the goal direction and the nearest axis-aligned direction in the λ^* -box. Bug2 is complete for simply-connected obstacles in the plane [8]. Our modification preserves this provided $\lambda^* > 0$ at every reachable configuration. If $\lambda^* = 0$ (kinematic singularity or exhausted joint limits), the planner reports infeasibility.

2) *Adaptive Step Size*: At each step t , compute $\lambda^*(\boldsymbol{\theta}^{(t)})$ from (22). The Cartesian displacement is then

$$\Delta \mathbf{z}^{(t)} = \text{clip}(\alpha \lambda^* \cdot \mathbf{d}^{(t)}, -\lambda^*, \lambda^*), \quad (28)$$

where $\mathbf{d}^{(t)}$ is the unit direction (toward goal in GTG, tangential in BF), $\alpha \in (0, 1)$ is a conservatism factor, and clip denotes component-wise clamping.

3) *Joint Update via Polynomial IK*: The joint update uses the second-order polynomial (11):

$$\boldsymbol{\theta}^{(t+1)} = \hat{\boldsymbol{\theta}}(\Delta \mathbf{z}^{(t)}). \quad (29)$$

By Theorem 1, since $\Delta \mathbf{z}^{(t)} \in [-\lambda^*, \lambda^*]^2$, the joint displacement satisfies (3) automatically.

The complete algorithm is given in Algorithm 1.

D. Efficient Implementation

While the SOS program (22) provides the theoretical foundation, solving the bilinear SDP at each planning step via a general-purpose NLP solver (e.g., Ipopt [19]) is computationally expensive.

We exploit the fact that the S-procedure matrix $S_{i,\sigma} \in \mathbb{S}^3$ (cf. (23)) is only 3×3 , so the certification problem has very low dimensionality. For a degree-2 polynomial over a box domain, the maximum of $|\Delta \hat{\theta}_i(\Delta \mathbf{z})|$ over $[-\lambda, \lambda]^2$

Algorithm 1 SOS-Verified Bug2 Planner

Require: $\boldsymbol{\theta}^{(0)}$, \mathbf{z}_{goal} , $\boldsymbol{\delta}$, \mathcal{O} , α , ϵ_{tol} , ρ

- 1: mode \leftarrow GTG; $\mathbf{z}^{(0)} \leftarrow \text{FK}(\boldsymbol{\theta}^{(0)})$
- 2: **for** $t = 0, 1, 2, \dots$ **do**
- 3: **if** $\|\mathbf{z}^{(t)} - \mathbf{z}_{\text{goal}}\| < \epsilon_{\text{tol}}$ **then**
- 4: **return** success
- 5: **end if**
- 6: Compute A, B via (6)–(10)
- 7: Compute $\varepsilon(\rho)$ via (12); set $\boldsymbol{\delta}^{\text{eff}}$ via (13)
- 8: Solve (22) $\Rightarrow \lambda^*$
- 9: **if** $\lambda^* < \epsilon_{\text{min}}$ **then**
- 10: Retry with smaller ρ
- 11: **end if**
- 12: Compute $\mathbf{d}^{(t)}$ (GTG or BF)
- 13: $\Delta \mathbf{z}^{(t)} \leftarrow \text{clip}(\alpha \lambda^* \mathbf{d}^{(t)}, -\lambda^*, \lambda^*)$
- 14: **if** $\mathbf{z}^{(t)} + \Delta \mathbf{z}^{(t)} \in \mathcal{O}$ **then**
- 15: Switch to BF; recompute $\Delta \mathbf{z}^{(t)}$
- 16: **end if**
- 17: $\boldsymbol{\theta}^{(t+1)} \leftarrow \hat{\boldsymbol{\theta}}(\Delta \mathbf{z}^{(t)})$ via (11)
- 18: $\mathbf{z}^{(t+1)} \leftarrow \text{FK}(\boldsymbol{\theta}^{(t+1)})$
- 19: **end for**

can be evaluated exactly on a sufficiently dense grid, since the optimizer lies at a vertex, edge extremum, or the unique interior critical point. This yields a bisection procedure: for each joint i , binary search on λ using the grid maximum as the feasibility oracle. With 50 bisection iterations and a 21×21 grid, the total cost is $n \times 50 \times 441 \approx 66,000$ floating-point operations per planning step, completing in sub-millisecond time.

Proposition 3 (Equivalence): For degree-2 polynomials over boxes, the bisection procedure computes the same λ^* as the SOS program (22), since the SOS relaxation is exact for quadratic polynomials over quadratic domains.

Proof: Fix joint i and sign $\sigma \in \{+1, -1\}$. For a given λ , the question of whether $\sigma \cdot \mathbf{y}^\top Q_i \mathbf{y} \leq \delta_i^{\text{eff}}$ for all $\Delta \mathbf{z} \in [-\lambda, \lambda]^2$ can be lifted to a semidefinite program by introducing $Y = \mathbf{y} \mathbf{y}^\top \in \mathbb{S}^3$ and relaxing $Y = \mathbf{y} \mathbf{y}^\top$ to $Y \succeq 0$:

$$\begin{aligned} p^* &= \max \text{tr}(\sigma Q_i \cdot Y) \\ \text{s.t. } & Y_{00} = 1, Y_{11} \leq \lambda^2, Y_{22} \leq \lambda^2, Y \succeq 0. \end{aligned}$$

The Lagrangian dual of this SDP, with multipliers ν for $Y_{00} = 1$ and $\mu_1, \mu_2 \geq 0$ for the box constraints, yields precisely the S-procedure certificate (21) upon identifying $\nu = \delta_i^{\text{eff}}$ and $\mu_k = c_k$.

Strong duality: Slater’s condition holds for the primal SDP (e.g., $Y = \frac{1}{2} \lambda^2 I$ is strictly feasible for sufficiently small scaling), so the primal and dual optima coincide.

SDP exactness: The primal has a 3×3 matrix variable with $m = 3$ affine constraints. By the Pataki–Barvinok rank bound [20], any optimal Y^* satisfies $r(r+1)/2 \leq m = 3$, giving $r \leq 1$. Since rank-1 feasible points exist (any \mathbf{y} in the box gives $Y = \mathbf{y} \mathbf{y}^\top$), the optimum is attained at rank 1, i.e., $Y^* = \mathbf{y}^*(\mathbf{y}^*)^\top$. Thus the SDP relaxation is exact: p^* equals the true maximum of $\sigma \cdot \mathbf{y}^\top Q_i \mathbf{y}$ over the box.

Combining: the true maximum = p^* (SDP exactness) = dual optimal (strong duality) = S-procedure bound. Therefore the S-procedure certifies $\sigma \cdot \Delta \hat{\theta}_i \leq \delta_i^{\text{eff}}$ over $[-\lambda, \lambda]^2$ if and only if the constraint holds. Since both the bisection and the SOS program find the largest λ for which all $2n$ constraints hold, they return the same λ^* . ■

V. EXPERIMENTS

We design our experiments to answer two research questions:

RQ1: Does the SOS-verified planner eliminate joint-limit violations compared to a standard Bug2 planner, and does this advantage persist across a range of joint-limit settings?

RQ2: Does preventing violations improve task-level outcomes—goal-reaching success, path quality, and tracking accuracy—or merely trade safety for performance?

A. Experimental Setup

1) *Task Setting:* We evaluate on a planar 3-link revolute manipulator ($n = 3$) with link lengths $l_1 = 1.0$, $l_2 = 0.8$, $l_3 = 0.6$ m. A single circular obstacle with radius $r = 0.015$ m is placed along the direct start–goal path to force boundary-following through kinematically challenging regions. The goal tolerance is $\epsilon_{\text{tol}} = 0.005$ m and the obstacle safety margin is 0.008 m.

To ensure a comprehensive evaluation, we test six uniform per-step joint bounds $\delta \in \{0.020, 0.025, 0.030, 0.035, 0.040, 0.050\}$ rad, spanning tight to moderate constraints. For each δ , we generate a pool of *adversarial scenarios* via an automated search (described below) and collect up to 100 scenarios per setting.

2) *Adversarial Scenario Generation:* We require scenarios where vanilla Bug2 is *guaranteed* to violate joint limits while the SOS planner can succeed. Each candidate scenario ($\theta_0, z_{\text{goal}}$) is accepted only if all of the following hold: (i) the starting condition number satisfies $2.5 \leq \kappa_0 \leq 8.0$ (moderate, not degenerate); (ii) $\kappa(J)$ increases by a ratio $\geq 1.6\times$ along the straight-line path (ensuring the vanilla step $s = \delta/\kappa_0$ eventually violates); (iii) $\lambda^* > 0$ at every sampled point on the path (the SOS planner can traverse the full distance); (iv) the estimated step count $\|\Delta z\|/(0.75 \cdot \lambda_{\text{min}}^*) < 500$ (the SOS planner finishes within budget); (v) vanilla Bug2, when run, incurs at least one joint-limit violation. Scenarios that pass all five filters are retained.

3) Planners Under Comparison:

a) *Vanilla Bug2 (baseline):* Fixed Cartesian step $s = \delta/\kappa_0$. Joint displacements are computed via the first-order pseudoinverse $\Delta \theta = J^\dagger \Delta z$. When $\|\Delta \theta\|_\infty > \delta$, each joint increment is *clipped* to $[-\delta, \delta]$, modeling a realistic actuator that respects physical limits. Maximum budget: 500 steps.

b) *SOS-Verified Bug2 (ours):* Adaptive step $s^{(t)} = 0.75 \cdot \lambda^*(\theta^{(t)})$. Joint displacements via the second-order polynomial IK (11). The polynomial approximation uses $\rho = 0.008$ for error estimation; if $\lambda^* < 10^{-6}$, ρ is halved iteratively (up to 3 retries). If a joint bound is marginally exceeded due to numerics, the step is scaled back by a factor $0.9 \cdot \min_i(\delta_i/|\Delta \theta_i|)$. Maximum budget: 600 steps.

TABLE I: Scenario metadata across joint-limit settings

δ (rad)	N	κ_0 (mean \pm std)	κ ratio (mean \pm std)
0.020	22	3.71 \pm 0.13	1.67 \pm 0.04
0.025	16	3.79 \pm 0.16	1.70 \pm 0.07
0.030	9	3.73 \pm 0.13	1.69 \pm 0.05
0.035	15	3.80 \pm 0.13	1.71 \pm 0.05
0.040	11	3.76 \pm 0.15	1.66 \pm 0.05
0.050	21	3.77 \pm 0.12	1.67 \pm 0.05

TABLE II: Joint-limit violations: count and rate (mean \pm std, best in **bold**)

δ	Violation Count		Violation Rate (%)	
	Vanilla	SOS	Vanilla	SOS
0.020	2.3 \pm 1.5	0.0 \pm 0.0	6.51 \pm 4.07	0.0 \pm 0.0
0.025	2.4 \pm 1.8	0.0 \pm 0.0	8.18 \pm 5.66	0.0 \pm 0.0
0.030	3.0 \pm 1.6	0.0 \pm 0.0	8.46 \pm 4.17	0.0 \pm 0.0
0.035	3.5 \pm 3.2	0.0 \pm 0.0	9.14 \pm 4.39	0.0 \pm 0.0
0.040	5.0 \pm 5.1	0.0 \pm 0.0	8.42 \pm 4.66	0.0 \pm 0.0
0.050	6.9 \pm 5.3	0.0 \pm 0.0	11.24 \pm 5.51	0.0 \pm 0.0

4) *Evaluation Metrics:* We report the following metrics, each averaged over all scenarios within a δ setting:

- **Success rate (%)**: fraction of scenarios reaching the goal within budget.
- **Violation count**: number of steps where $\max_i |\Delta \theta_i| > \delta$ (pre-clip for vanilla, pre-scale-back for SOS).
- **Violation rate (%)**: violation count divided by total steps.
- **Final distance**: $\|z_{\text{final}} - z_{\text{goal}}\|$ at termination.
- **Path length ratio**: total end-effector path length divided by straight-line distance (1.0 is optimal).

B. Statistical Comparison

Table I summarizes the scenario difficulty. Across all δ settings, the starting condition number averages $\kappa_0 \approx 3.8$ with a κ ratio (max/start) of $\approx 1.7\times$. The total number of retained scenarios ranges from 9 to 22 per δ (94 total across all settings), reflecting the stringent five-part acceptance criterion.

1) *Joint-Limit Violations:* Table II presents the core safety metric. The SOS-verified planner achieves **zero** violations in every scenario at every δ setting, confirming the theoretical guarantee of Theorem 1. In contrast, vanilla Bug2 incurs 2–7 violations per scenario on average, with the violation rate increasing from 6.5% at $\delta = 0.020$ to 11.2% at $\delta = 0.050$. Larger δ makes the fixed step δ/κ_0 more aggressive, amplifying the mismatch in high- κ regions.

2) *Goal-Reaching Success and Path Quality:* Table III reports success rate, final distance, and path efficiency. The SOS planner achieves **100% success** at all δ settings. Vanilla Bug2 reaches the goal reliably at tight limits ($\delta \leq 0.030$) because the small fixed step happens to be close to the safe threshold, but at looser limits ($\delta \geq 0.035$) its success rate drops to 82–93% as the larger step induces more clipping drift.

The path length ratio reveals a striking contrast. At $\delta = 0.020$ – 0.025 both planners follow near-optimal paths ($\approx 1.2\times$ straight-line). At $\delta = 0.040$ – 0.050 , vanilla Bug2’s drift

TABLE III: Success rate, final distance, and path length ratio (mean \pm std; best in **bold**)

δ	Success Rate (%)		Path Length Ratio	
	Vanilla	SOS	Vanilla	SOS
0.020	100.0	100.0	1.21 ± 0.02	1.17 ± 0.02
0.025	100.0	100.0	1.23 ± 0.02	1.18 ± 0.02
0.030	100.0	100.0	1.94 ± 1.05	1.20 ± 0.01
0.035	93.3	100.0	3.85 ± 7.48	1.21 ± 0.02
0.040	81.8	100.0	8.85 ± 13.0	1.22 ± 0.03
0.050	85.7	100.0	10.3 ± 15.2	1.47 ± 0.67

TABLE IV: Computational cost and step count (best in **bold**)

δ	Steps		Wall Time (s)	
	Vanilla	SOS	Vanilla	SOS
0.020	35.3	52.4	<0.001	0.018
0.025	29.4	43.3	<0.001	0.014
0.030	38.3	36.4	<0.001	0.012
0.035	64.9	33.1	<0.001	0.011
0.040	126.8	28.1	<0.001	0.010
0.050	113.8	27.1	<0.001	0.009

inflates the path to 8.8–10.3 \times straight-line, while the SOS planner maintains a ratio of ≈ 1.2 –1.5 \times .

3) *Computational Cost*: The SOS-verified planner averages 0.009–0.018 s per scenario (Table IV), corresponding to ≈ 0.3 ms per planning step using the bisection procedure. Vanilla Bug2 is faster (< 0.001 s) since it performs only a matrix–vector multiply per step, but the SOS planner’s sub-millisecond overhead is well within real-time requirements for typical manipulation tasks.

An important observation is that for $\delta \geq 0.030$, the SOS planner actually uses *fewer steps* than vanilla Bug2. This is because vanilla’s clipping-induced drift causes it to wander off the intended path, requiring many corrective steps, whereas the SOS planner follows a direct, drift-free trajectory.

C. Qualitative Analysis

Fig. 2 illustrates a representative scenario with $\delta = 0.035$ rad, $\kappa_0 = 6.4$, and $\kappa_{\max} = 34.2$ (5.3 \times ratio). The path difference visible in Fig. 2 is *not* due to randomness or backtracking—Bug2 is a deterministic algorithm. The cause is clipping-induced drift. When the vanilla planner’s pseudoinverse IK requests a joint displacement that exceeds δ , the displacement is clipped to $[-\delta, \delta]$. The actual end-effector position after clipping differs from what the planner intended, so at the next step the planner computes the goal direction from a *different* current position. This drift accumulates: each clipped step shifts the starting point of the next, producing a trajectory that progressively deviates from the intended path. The SOS-verified planner, by contrast, never clips—every step lands exactly where intended—so it follows the straight go-to-goal / boundary-follow path that Bug2 would follow in an ideal (unconstrained) setting.

a) *Cartesian paths (top row)*.: The vanilla planner’s path (top-left) shows red segments where joint limits were violated and subsequently clipped, producing visible kinks. The SOS planner (top-right) follows a smooth path; the

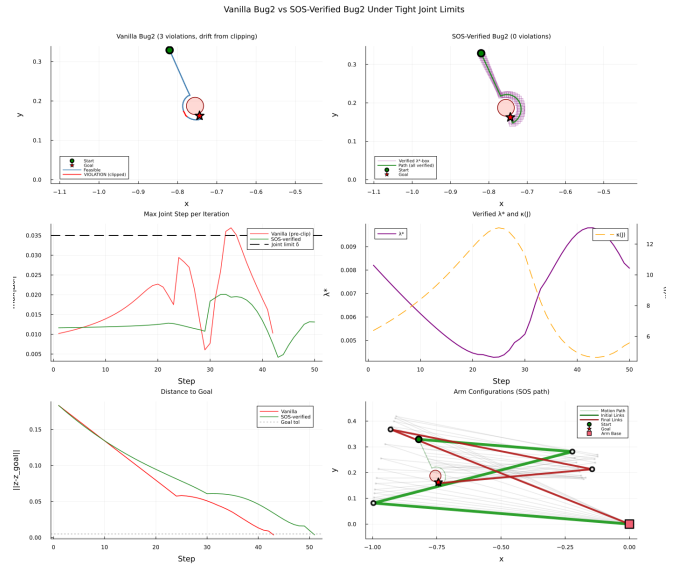


Fig. 2: Comparison of Vanilla Bug2 (left) and SOS-Verified Bug2 (right). **Top**: Cartesian paths; red segments mark steps where joint limits were violated and clipped (vanilla only), causing the trajectory to deviate from the SOS path. Purple boxes show the certified λ^* -regions. The two planners follow *different* paths because clipping shifts vanilla’s current position at each violated step, altering subsequent Bug2 direction decisions (see text for details). **Middle-left**: Max joint step per iteration; the dashed line is $\delta = 0.035$. **Middle-right**: λ^* (purple) and $\kappa(J)$ (orange); note the inverse relationship. **Bottom**: Distance to goal and sampled arm configurations.

purple rectangles show the λ^* -boxes, which visibly shrink near the obstacle where $\kappa(J)$ peaks.

b) *Joint-step compliance (middle-left)*.: The vanilla planner’s pre-clip joint deviations (red) exceed the dashed δ -line at three points. The SOS planner’s deviations (green) remain strictly below the limit throughout.

c) *Adaptive λ^* (middle-right)*.: The purple curve shows λ^* dropping from 0.008 to 0.005 as $\kappa(J)$ (orange dashed) rises from 6 to 12, then recovering. This adaptation is the mechanism by which the planner avoids violations without any explicit joint-limit checking in the planning loop.

d) *Arm configurations (bottom-right)*.: Sampled arm poses along the SOS path show smooth, continuous motion with no abrupt reconfigurations.

D. Discussion

a) *Answering RQ1*.: The SOS-verified planner achieves zero joint-limit violations across *all* 94 adversarial scenarios and *all* six δ settings, while vanilla Bug2 violates limits in 6–11% of steps. The advantage is consistent and grows with δ .

b) *Answering RQ2*.: Eliminating violations does not sacrifice performance; it improves it. At $\delta \geq 0.035$, the SOS planner achieves higher success rates (100% vs. 82–93%), shorter paths (1.2 \times vs. 4–10 \times straight-line), and fewer steps (27–33 vs. 65–127). The only cost is a modest computational overhead of ≈ 0.3 ms per step, which is negligible for typical planning rates.

VI. CONCLUSION

We have presented an approach to task-space reactive motion planning that provides formal joint-feasibility guarantees at every planning step. By computing a certified Cartesian reachable set via SOS programming and using it to adaptively size the steps of a Bug2 planner, we eliminate the joint-limit violations and tracking drift that arise from fixed-step approaches. A statistical evaluation across 94 adversarial scenarios and six joint-limit settings confirms the theoretical guarantees: the SOS-verified planner achieves zero joint violations and 100% goal reaching in all cases, whereas vanilla Bug2 violates limits in 6–11% of steps and fails to reach the goal in up to 18% of scenarios at looser joint bounds. Crucially, eliminating violations does not degrade performance; it improves path quality and reduces step count by avoiding clipping-induced drift. Future work will extend the evaluation to higher-DOF systems, integrate with sampling-based planners (e.g., RRT) for complex 3D environments, and explore online adaptation of the polynomial approximation order.

REFERENCES

- [1] B. Siciliano, L. Sciavicco, L. Villani, and G. Oriolo, *Robotics: modelling, planning and control*. Springer, 2009.
- [2] S. M. LaValle, *Planning algorithms*. Cambridge university press, 2006.
- [3] M. Stilman, “Global manipulation planning in robot joint space with task constraints,” *IEEE Transactions on Robotics*, vol. 26, no. 3, pp. 576–584, 2010.
- [4] Z. Kingston, M. Moll, and L. E. Kavraki, “Sampling-based methods for motion planning with constraints,” *Annual review of control, robotics, and autonomous systems*, vol. 1, no. 1, pp. 159–185, 2018.
- [5] J. Schulman, J. Ho, A. X. Lee, I. Awwal, H. Bradlow, and P. Abbeel, “Finding locally optimal, collision-free trajectories with sequential convex optimization,” in *Robotics: science and systems*, vol. 9, no. 1. Berlin, Germany, 2013, pp. 1–10.
- [6] C. Liu, C.-Y. Lin, and M. Tomizuka, “The convex feasible set algorithm for real time optimization in motion planning,” *SIAM Journal on Control and optimization*, vol. 56, no. 4, pp. 2712–2733, 2018.
- [7] J. Colan, A. Davila, and Y. Hasegawa, “Variable step sizes for iterative jacobian-based inverse kinematics of robotic manipulators,” *IEEE Access*, vol. 12, pp. 87 909–87 922, 2024.
- [8] V. J. Lumelsky and A. A. Stepanov, “Path-planning strategies for a point mobile automaton moving amidst unknown obstacles of arbitrary shape,” *Algorithmica*, vol. 2, no. 1, pp. 403–430, 1987.
- [9] R. Tedrake, I. R. Manchester, M. Tobenkin, and J. W. Roberts, “Lqr-trees: Feedback motion planning via sums-of-squares verification,” *The International Journal of Robotics Research*, vol. 29, no. 8, pp. 1038–1052, 2010.
- [10] A. Majumdar and R. Tedrake, “Funnel libraries for real-time robust feedback motion planning,” *The International Journal of Robotics Research*, vol. 36, no. 8, pp. 947–982, 2017.
- [11] P. A. Parrilo, “Semidefinite programming relaxations for semialgebraic problems,” *Mathematical programming*, vol. 96, no. 2, pp. 293–320, 2003.
- [12] V. A. Yakubovich, “S-procedure in nonlinear control theory,” *Vestnik Leningradskogo Universiteta, Ser. Matematika*, pp. 62–77, 1971.
- [13] I. Pólik and T. Terlaky, “A survey of the s-lemma,” *SIAM review*, vol. 49, no. 3, pp. 371–418, 2007.
- [14] Z. Kingston, M. Moll, and L. E. Kavraki, “Exploring implicit spaces for constrained sampling-based planning,” *The International Journal of Robotics Research*, vol. 38, no. 10-11, pp. 1151–1178, 2019.
- [15] T. Marcucci, M. Petersen, D. Von Wrangel, and R. Tedrake, “Motion planning around obstacles with convex optimization,” *Science robotics*, vol. 8, no. 84, p. eadf7843, 2023.
- [16] C. W. Wampler, “Manipulator inverse kinematic solutions based on vector formulations and damped least-squares methods,” *IEEE Transactions on Systems, Man, and Cybernetics*, vol. 16, no. 1, pp. 93–101, 2007.
- [17] Y. Nakamura and H. Hanafusa, “Inverse kinematic solutions with singularity robustness for robot manipulator control,” 1986.
- [18] O. Khatib, “Real-time obstacle avoidance for manipulators and mobile robots,” *The international journal of robotics research*, vol. 5, no. 1, pp. 90–98, 1986.
- [19] A. Wächter and L. T. Biegler, “On the implementation of an interior-point filter line-search algorithm for large-scale nonlinear programming,” *Mathematical programming*, vol. 106, no. 1, pp. 25–57, 2006.
- [20] A. I. Barvinok, “Problems of distance geometry and convex properties of quadratic maps,” *Discrete & Computational Geometry*, vol. 13, no. 2, pp. 189–202, 1995.